

SM8: Summer Temperature Inferences

ST1 Calibration and Reconstructions (Figures ST01 to ST06)

ST1 Calibration and Reconstructions

As discussed in the main text, we calibrate the chronologies separately for the two frequency bands: those exhibiting variations on timescales less than 15 years (high frequency) and between 15 and 100 years (medium frequency). The variations on timescales greater than 100 years (low frequency) cannot be directly calibrated because there are insufficient degrees of freedom on this timescale given the 123-year instrumental temperature record; such a calibration would amount to scaling the series so that the trends had the same amplitude. Instead the scaling factor used to calibrate the 15–100-year data is also applied to the >100-year data.

We also combine the available data in multiple ways to make best use of the most reliable information, as explained in the main text. For the longest period (96 BCE to 2005 CE), using only the Yamal TRW chronology (rather than the combined Yamalia chronology) provides the most homogeneous measure of tree-growth in the region. We calibrate the high and medium frequency variations separately because TRW autocorrelation can suppress the magnitude response to the short-term temperature excursions and result in a different optimal scaling factor at these timescales.

If we restrict our interest to the last millennium, the high-frequency information contained in the Polar Urals MXD chronology can be utilized. Despite the reduced replication of this chronology prior to 1850, and particularly prior to 1600, the chronology confidence (represented by the standard error of the mean of the individual sample values in each year in the main paper, but consistent with the ‘adjusted’ EPS metric and bootstrap estimates of uncertainty explored in SM6) indicates that the high-frequency common signal is still strong throughout most of the millennium. The MXD chronology confidence is much reduced on timescales longer than 15 years and we contend that the replication is insufficient prior to 1600 to provide a more reliable representation of growth changes on those timescales than the much better replicated Yamal or Yamalia TRW chronologies. Consequently, we combine the calibrated high-frequency Polar Urals MXD with the calibrated Yamalia TRW data for the medium and low frequencies to form a Yamalia summer temperature reconstruction for the 914 to 2005 CE period.

For both the Yamal TRW and the Yamalia combined TRW and MXD reconstructions, each medium-frequency TRW series can be calibrated against the band-pass (15–100 year) filtered summer temperature data. There are, however, rather few degrees of freedom in this band-pass series within the 123-year calibration period and this will be reflected in higher uncertainty in the calibration scaling factor (this uncertainty is not quantified here, though we do report the uncertainty arising from the choice of regression method used to estimate the scaling factor; Table 2 of the main text). The availability of the MXD data provides an additional option for the calibration of the Yamalia TRW chronology. The MXD chronology has a strong correlation with the medium-frequency as well as the high-frequency variations in summer temperature (see also SM7 Figures CA04 and CA05), and so a single calibration of the MXD chronology on timescales shorter than 100 years is reasonable. This calibration, being based on variations on all timescales shorter than 100 years, has considerably more degrees of freedom and reduced uncertainty than a

medium-frequency calibration. We then have a *calibrated* MXD-based temperature history that is relatively reliable at medium (and more so at high) frequencies from 1600 CE onwards (prior to this the replication is too low), and we use this to calibrate the Yamalia medium-frequency TRW chronology using the full 406-year overlap (1600–2005). During this overlap, the two medium-frequency chronologies are well correlated ($r = 0.83$). As before, the calibration scaling factor determined for the medium-frequency TRW is also used to scale the low-frequency TRW chronology band.

Based on empirical correlations (see SM7 Table CA1 and Figure CA06), the most appropriate target season for the TRW chronologies is shorter (JJ) than for the MXD chronology (JJA). For the Yamalia combined chronology, we therefore explore four alternative reconstructions: with TRW calibrated directly against either JJ or JJA instrumental temperatures and with TRW calibrated indirectly against the calibrated MXD for either JJ or JJA. The greater degrees of freedom available in the indirect calibration is preferred, but it is dependent upon the accuracy of the calibrated MXD and this is likely to be less when the JJ target season is used because this is not optimal for the MXD data. The two preferred reconstructions, therefore, are those where the Yamalia TRW is calibrated directly against JJ instrumental temperature or against the JJA-calibrated MXD data. These are presented in the main text (Figure 12), together with the reconstruction based entirely on the Yamal TRW calibrated against JJ temperatures. The other two Yamalia reconstructions are shown here in this supplementary material.

The scaling factors used to “calibrate” the high and medium-frequency bands of each chronology are determined here by scaling the series so that its variance matches the variance of the instrumental record over the calibration period. In each case, the scaled series is then shifted by the addition of a constant so that its mean matches the instrumental record mean, again over the calibration period. The scaling factors obtained by this variance-matching method are compared with those obtained by temperature-on-chronology and chronology-on-temperature simple least-squares regression in Table 2 of the main text, and the relationship between these regression approaches is discussed in the main text.

All calibration is performed using the full overlap period between the instrumental record and the relevant chronology (1883–2005 for Yamal and 1883–2006 for Yamalia and Polar Urals), with the exception that some years from each end of the series are removed to reduce the influence of end effects on the filtered series. The high-frequency series are produced by high-pass filtering the measurement data with a 15-year spline and just two years are removed from each end. The medium-frequency series are band-passed using 15- and 100-year splines; the end effects associated with the latter are more significant and so 13 years are removed from each end.

The calibration data (after removal of end years) used in each case are shown in Figure ST01, with the tree-ring chronologies on the y-axis and the temperature data on the x-axis. The temperature-on-chronology, variance matching and chronology-on-temperature regression lines are indicated, together with the regression line equations (the inverse of the slopes are given in Table 2 of the main text).

The five reconstructions are shown in Figures ST02–ST06, illustrating variations and uncertainties for unfiltered (full) timeseries as well as for 15-year and 100-year smoothed time series. The residuals between the instrumental and reconstructed temperatures are also shown for each timescale. These residual series show small trends in most cases. These trends arise because we have made no attempt to fit the 100-year trend in the data; instead the amplitude of the 100-year trend in a reconstruction is determined by the trend in the tree-ring chronology multiplied by the scaling factor determined from the medium-frequency calibration. This provides a reasonable but not perfect fit, and in most cases shown here the reconstruction slightly overestimates the instrumental trend. Note additionally that the final decades of the 100-year filtered series are much more uncertain than shown because of the end effects of the spline filtering.

The uncertainties are estimated independently for each timescale by assuming the residuals between the instrumental temperature and the reconstructed temperature, at the timescale being considered, arise from a combination of “chronology uncertainty” and the “temperature representation uncertainty”. The former is estimated from the standard error of the mean of the individual sample values in each year (after the samples have been filtered to represent the timescale being considered) and varies from year-to-year. In particular, the chronology uncertainty shows long-term changes associated with changes in sample replication. This standard error is estimated for each frequency band separately and is scaled by the same factor (b_v) derived from the calibration of that frequency band, so that it represents an error in temperature units. The average of these year-by-year chronology standard errors ($b_v\sigma_C$) is calculated for the period of overlap with the instrumental temperature. The “temperature representation uncertainty” represents the uncertainty between the reconstruction and the instrumental temperature in the hypothetical case where the chronology has zero error (i.e. it is a perfect record of regional tree growth, obtained for example by using an infinite sample of trees, equivalent to $EPS = 1.0$). Even with a perfect record of regional tree growth, it will not be perfectly correlated with the specified summer temperature record because other factors (including temperature variations in other months) influence tree growth. This is the “temperature representation uncertainty” (σ_T) and is inferred by assuming that it can be combined in quadrature with the mean chronology uncertainty over the overlap period to obtain the standard deviation of the residuals (σ_R) at the timescales being considered:

$$\sigma_R^2 = b_v^2\sigma_C^2 + \sigma_T^2 \quad (\text{Equation ST1})$$

and therefore

$$\sigma_T = \sqrt{\sigma_R^2 - b_v^2\sigma_C^2}. \quad (\text{Equation ST2})$$

Having estimated σ_T in this manner (see Figures ST02–ST06 for the residuals calculated for each timescale calibration), we assume that it is time-invariant and that the time-varying chronology uncertainty expresses the deterioration of the reconstruction during periods with a weaker common signal or poorer replication. The time-varying overall reconstruction error is then obtained by Equation ST1 but now using the time-varying chronology uncertainty rather than its mean during the overlap period. The shading in Figures ST02–ST06 shows the different components of the overall reconstruction error with separate shading for the high versus the medium–low frequencies and the temperature representation uncertainty.

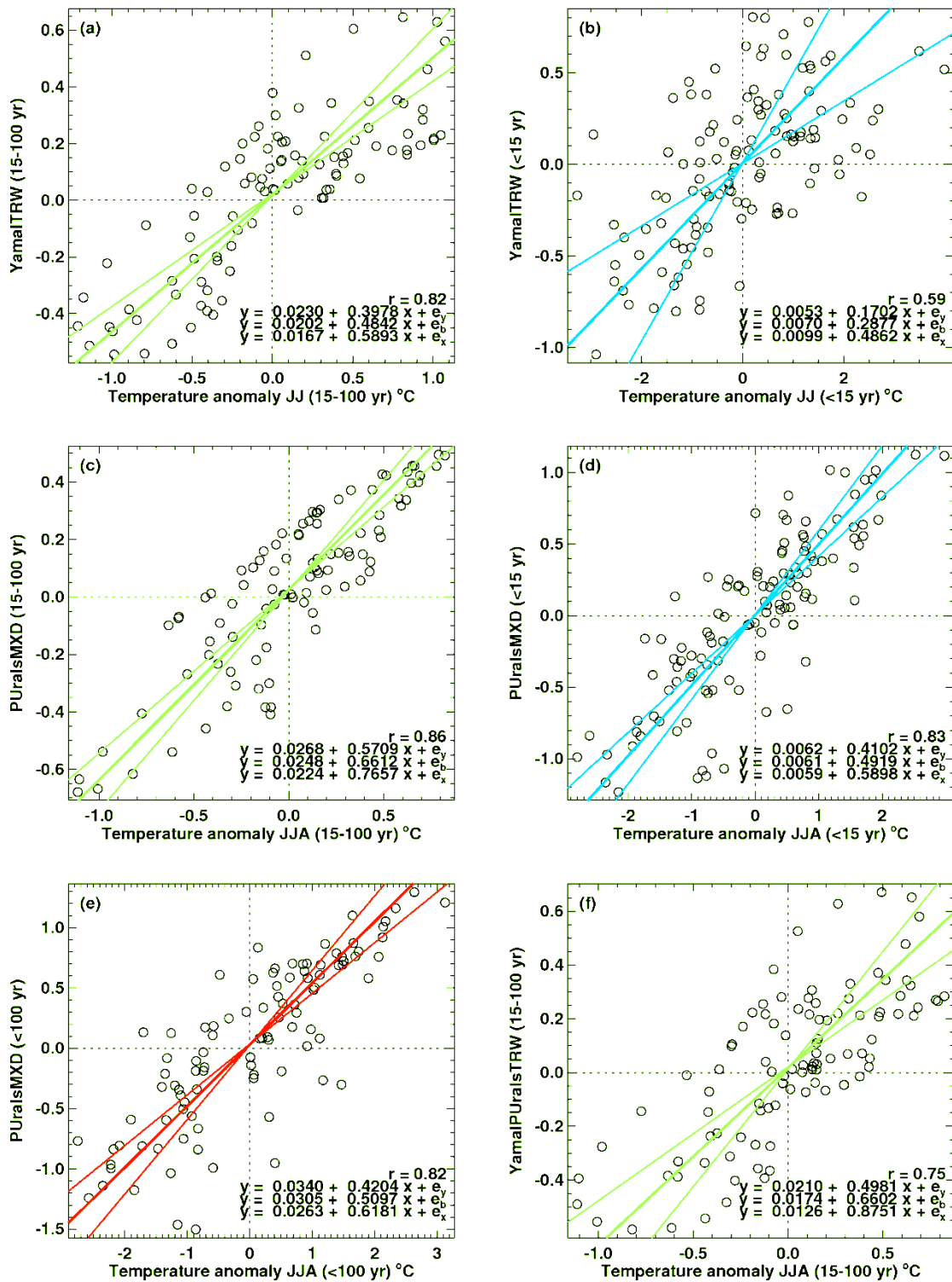


Figure ST01. Scatter plots and regression lines showing the calibration of the various chronologies, frequency bands and target seasonal temperatures: (a) Yamal TRW against JJ temperature for medium frequencies; (b) Yamal TRW against JJ temperature for high frequencies; (c) Polar Urals MXD against JJA temperature for medium frequencies; (d) Polar Urals MXD against JJA temperature for high frequencies; (e) Polar Urals MXD against JJA temperature for combined high and medium frequencies; (f) Yamalia TRW against JJA temperature for medium frequencies; (g–j) repeat of (c–f) but for JJ temperature.

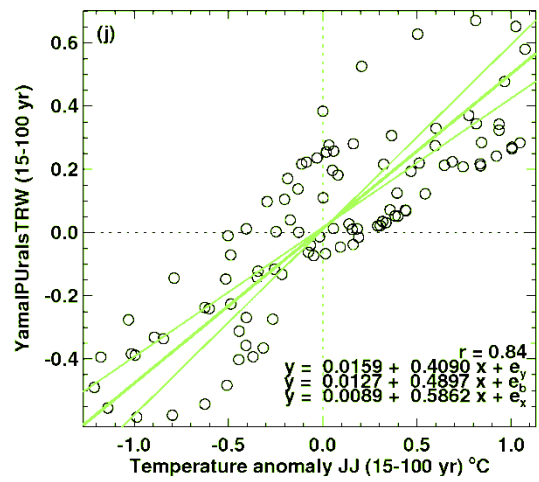
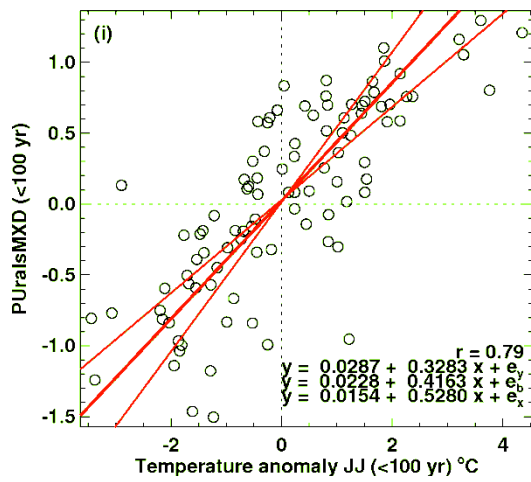
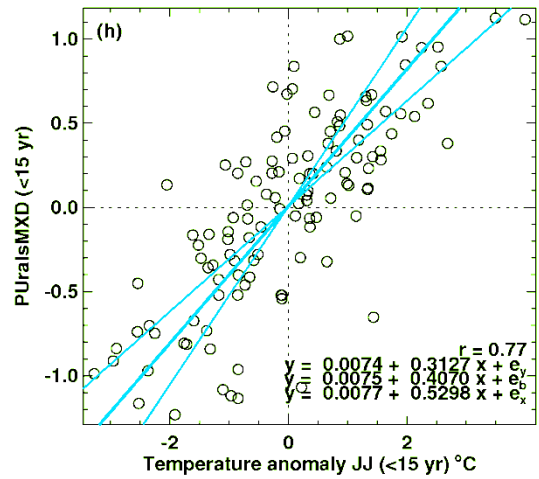
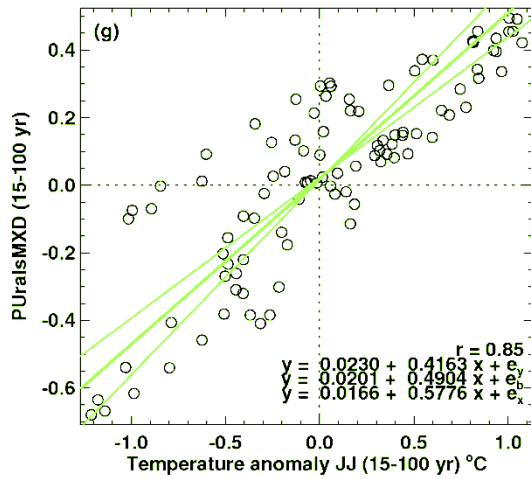


Figure ST01 (continued).

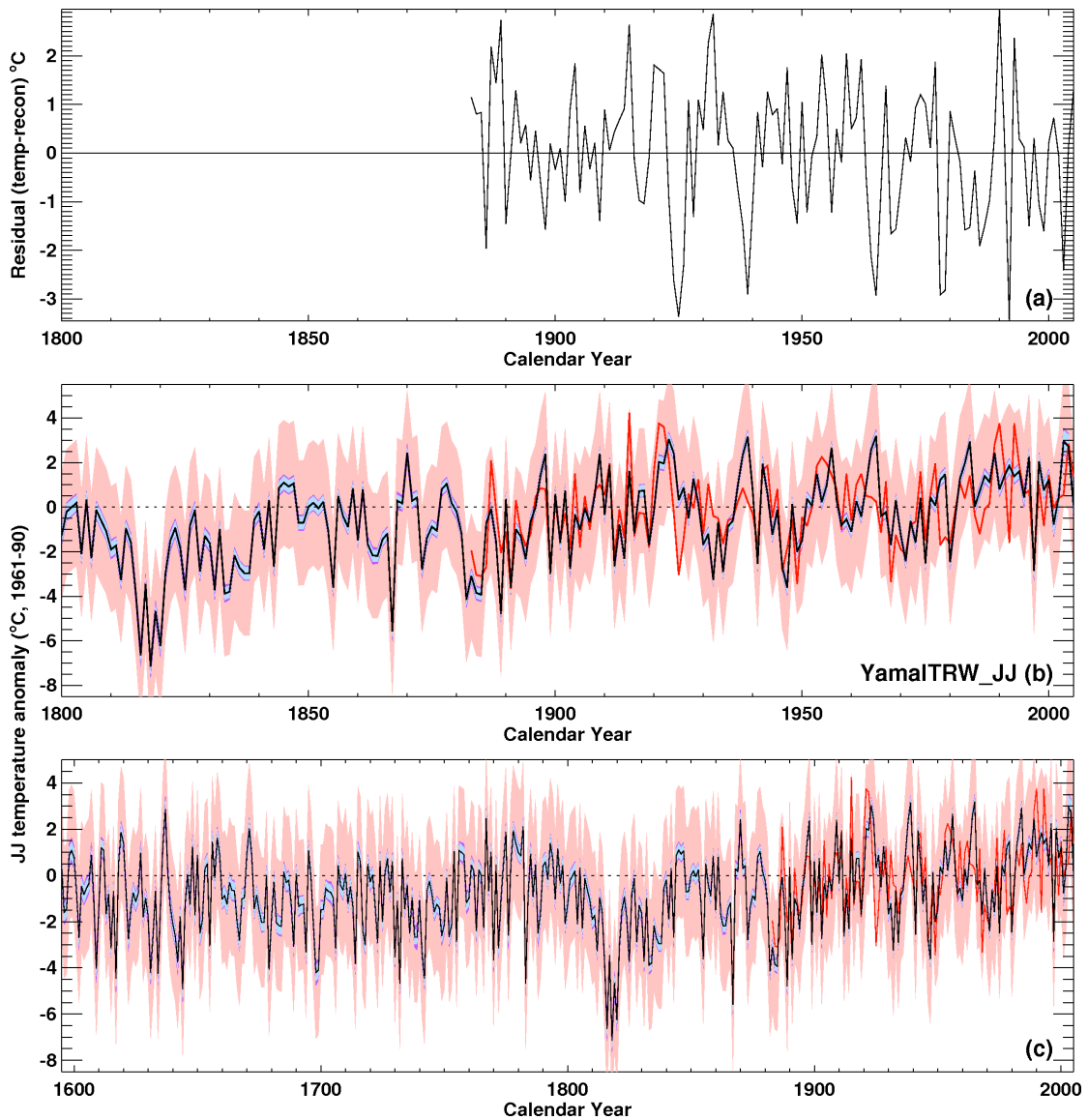


Figure ST02. The JJ temperature reconstruction based on the Yamal TRW chronology: (a) residual between full instrumental temperature and full reconstruction; (b) full reconstruction (black) together with chronology uncertainty (pale blue for combined medium and low-frequency uncertainty; dark purple for high-frequency uncertainty) and residuals uncertainty (pale red); (c) as (b) but for the longer 1595–2005 period; (d–e) as (a–b) but for timescales greater than 15 years; (f–g) as (a–b) but for timescales greater than 100 years. Uncertainty ranges are $\pm 2\sigma$.

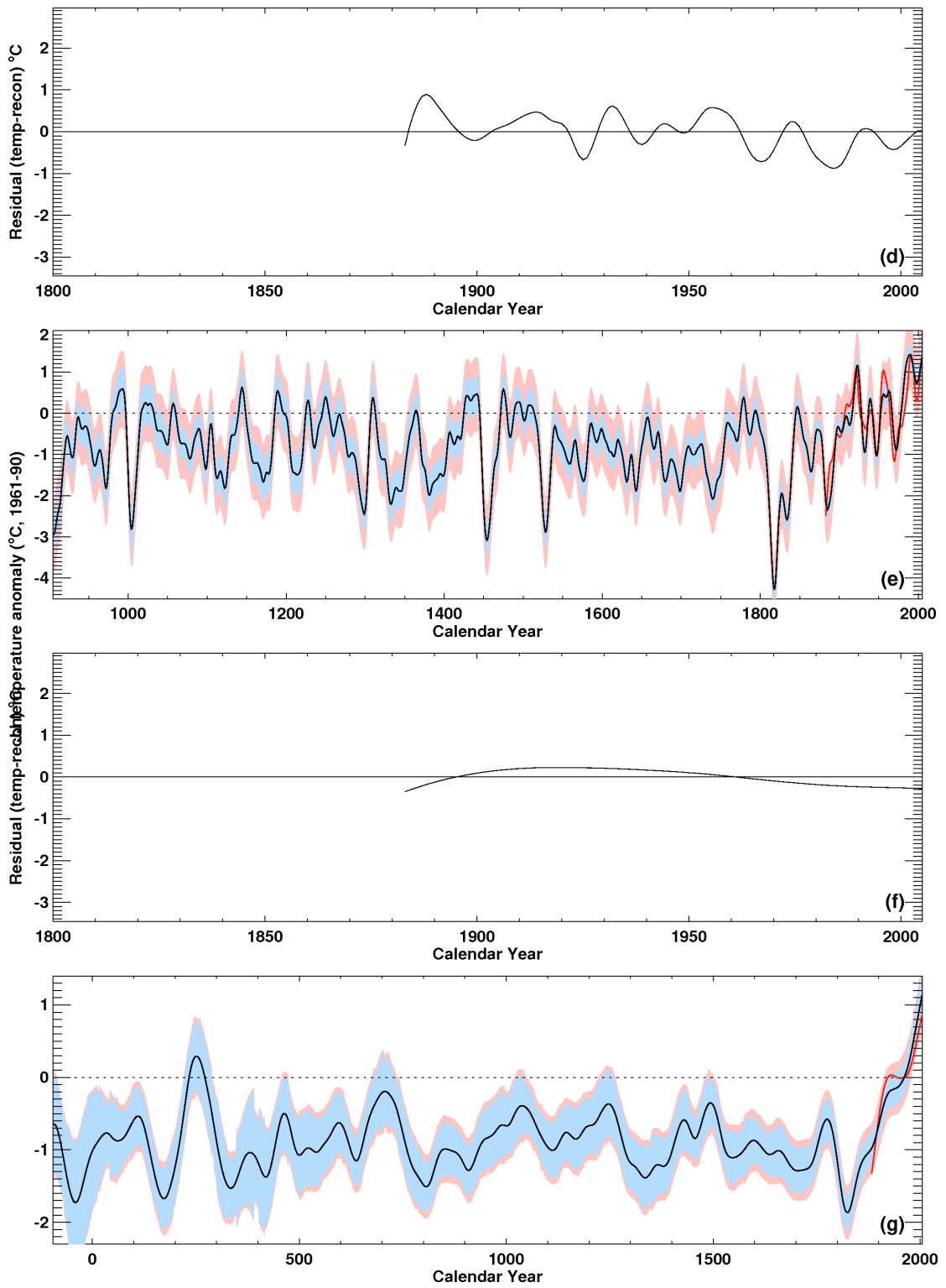


Figure ST02 (continued).

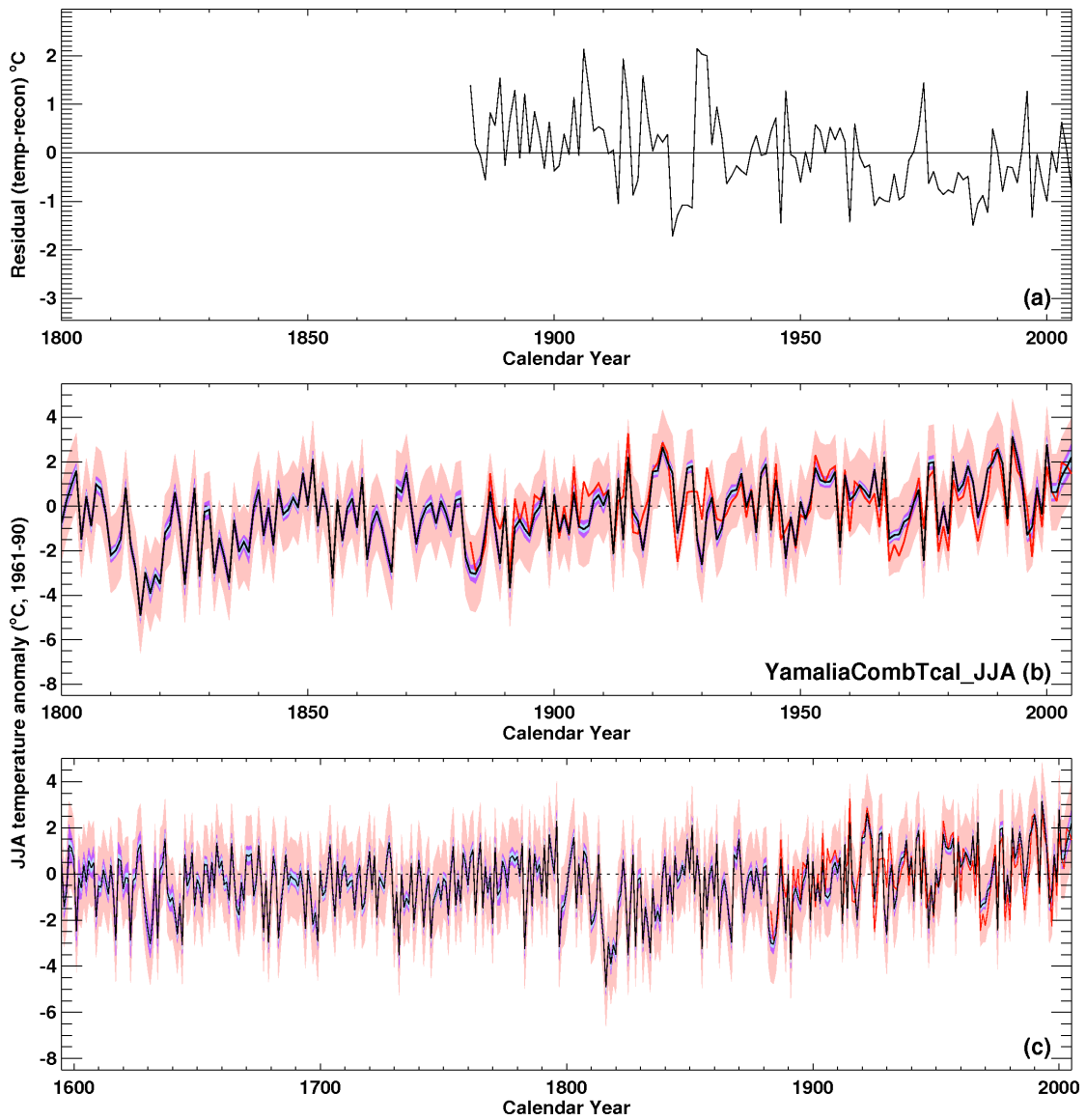


Figure ST03. As Figure ST02 but for the reconstruction of JJA temperature based on the high-frequency Polar Urals MXD chronology and the medium and low-frequency Yamalia TRW chronologies, with the medium-frequency TRW calibrated against instrumental temperature data.

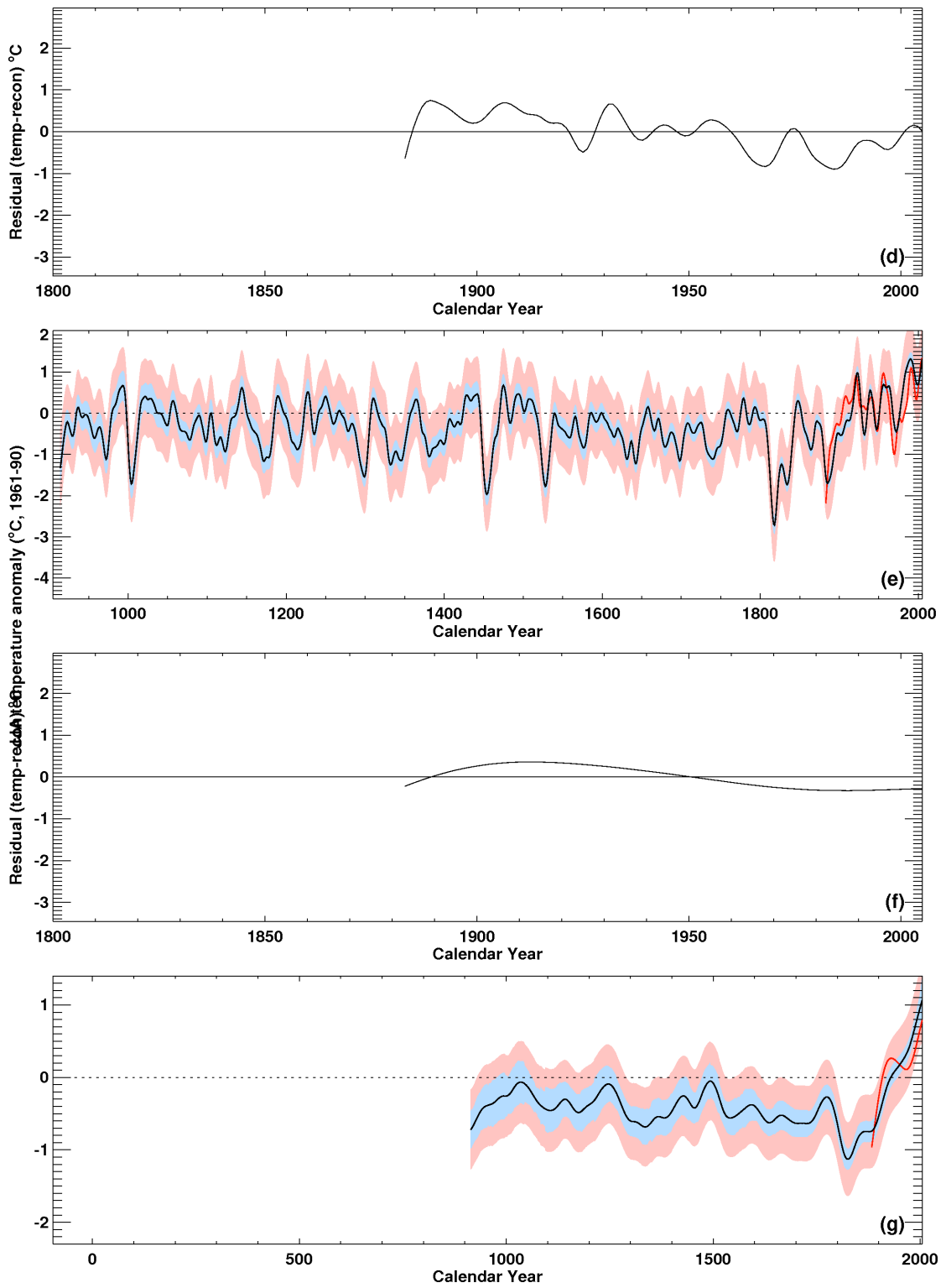


Figure ST03 (continued).

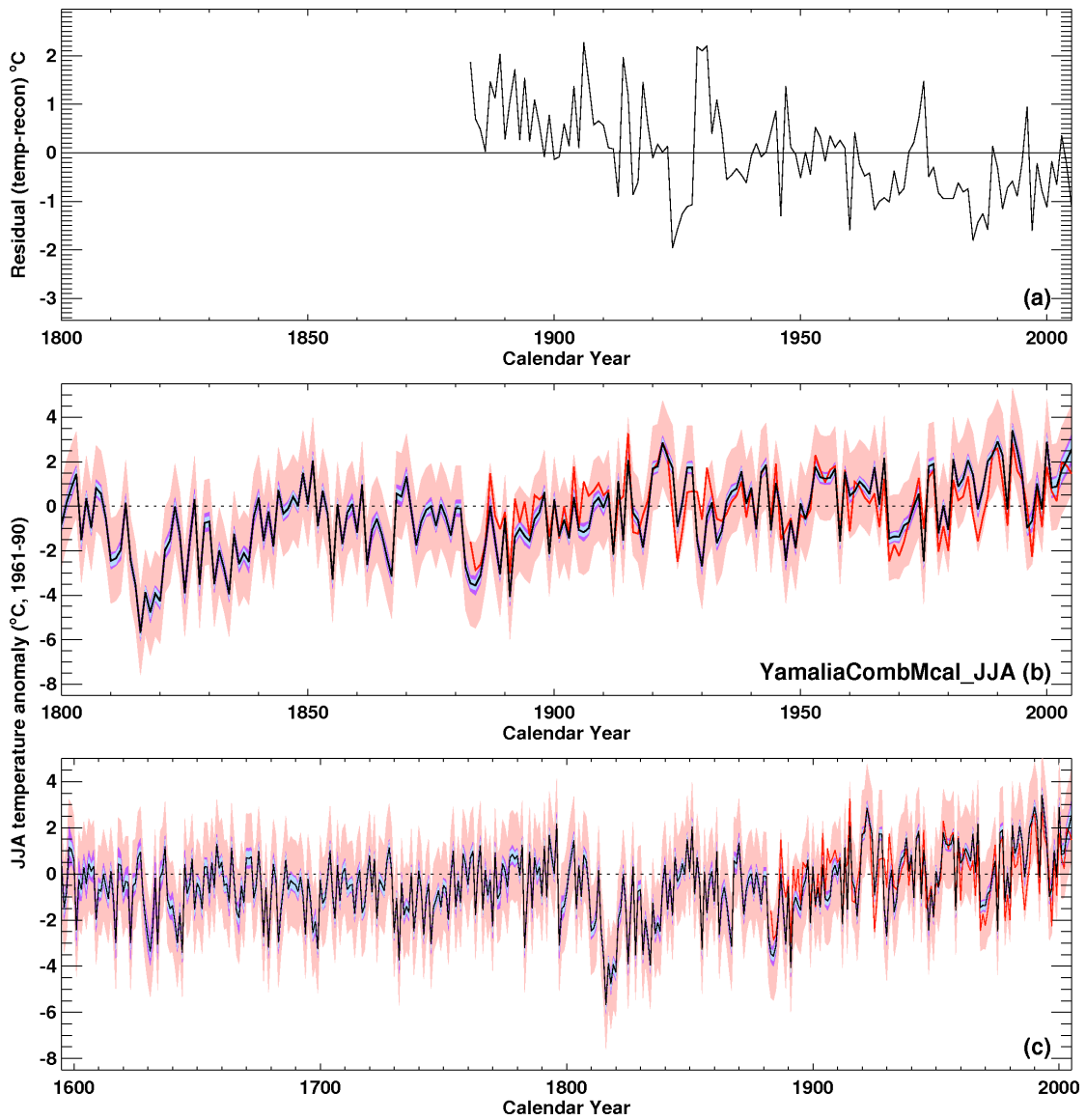


Figure ST04. As Figure ST02 but for the reconstruction of JJA temperature based on the high-frequency Polar Urals MXD chronology and the medium and low-frequency Yamalia TRW chronologies, with the medium-frequency TRW calibrated against calibrated medium-frequency MXD data.

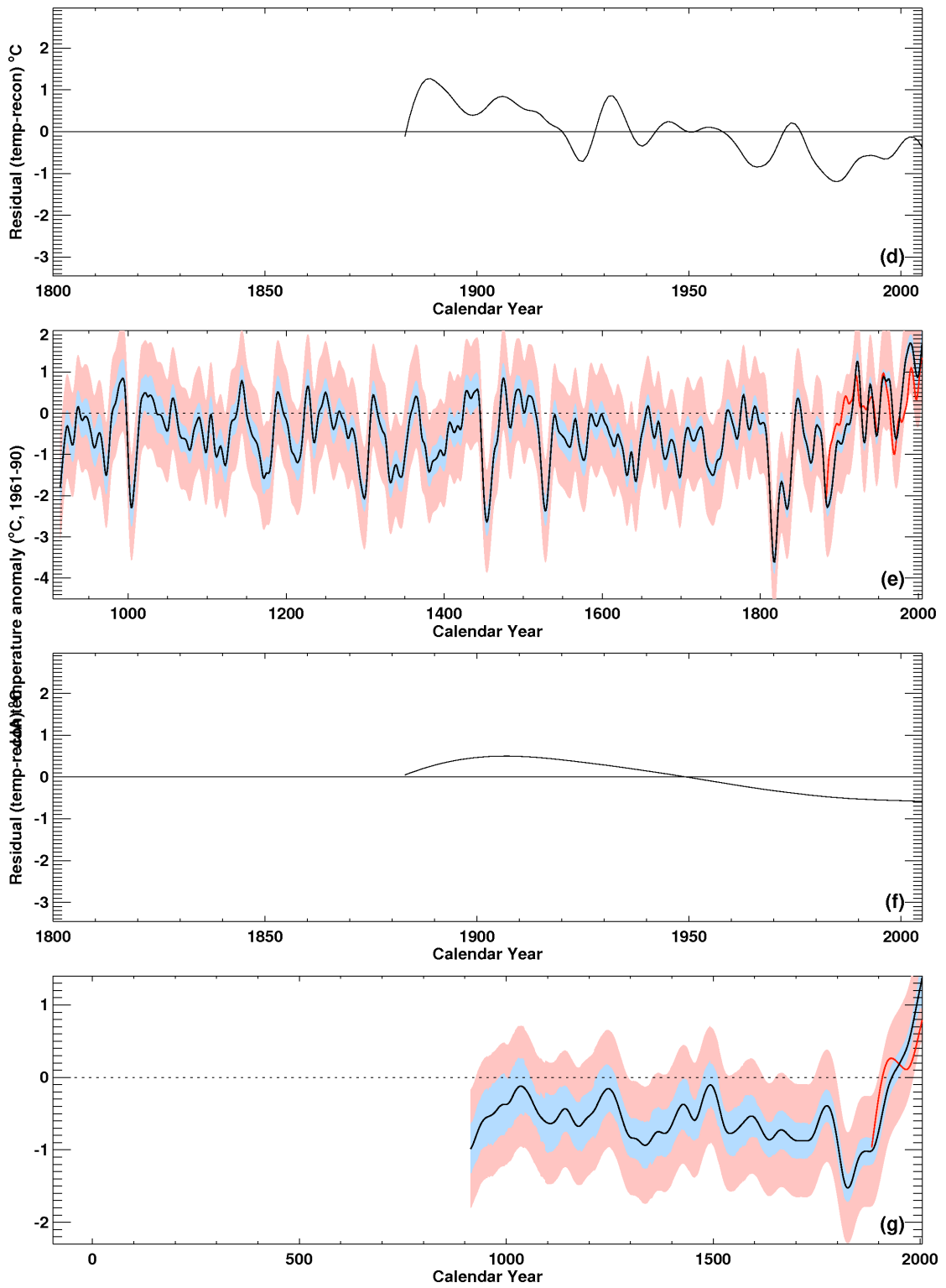


Figure ST04 (continued).

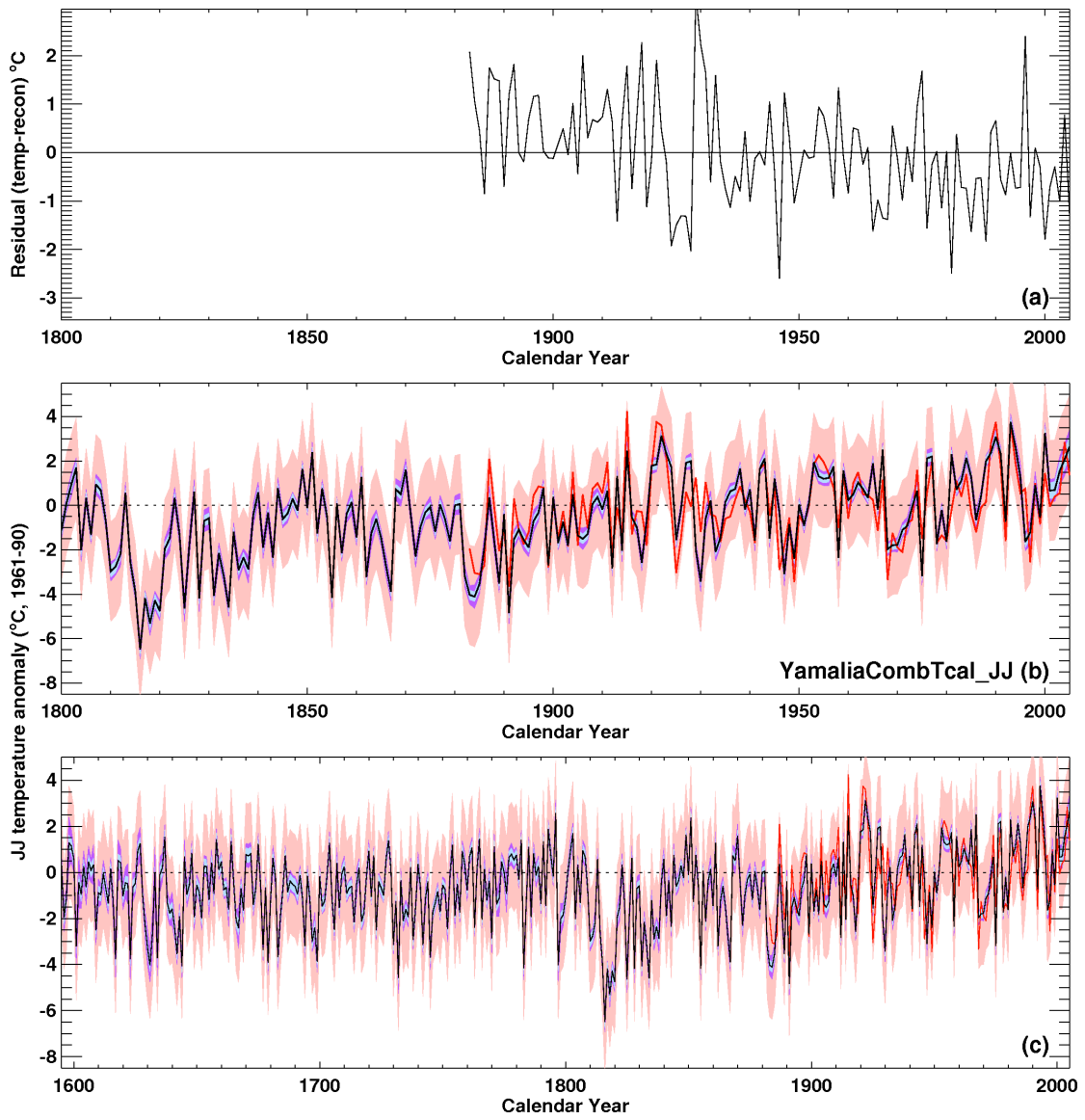


Figure ST05. As Figure ST03 but for JJ temperature.

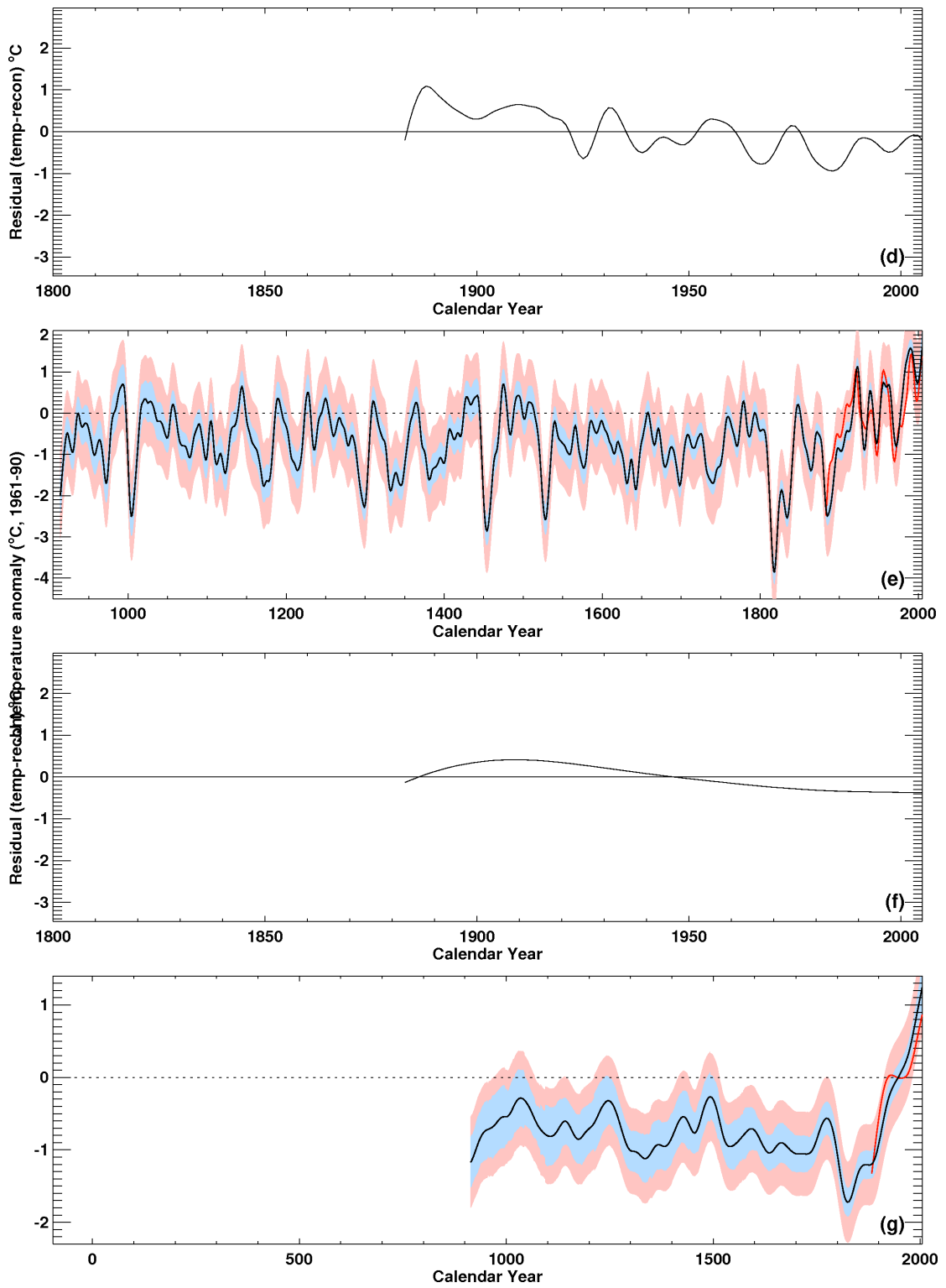


Figure ST05 (continued).

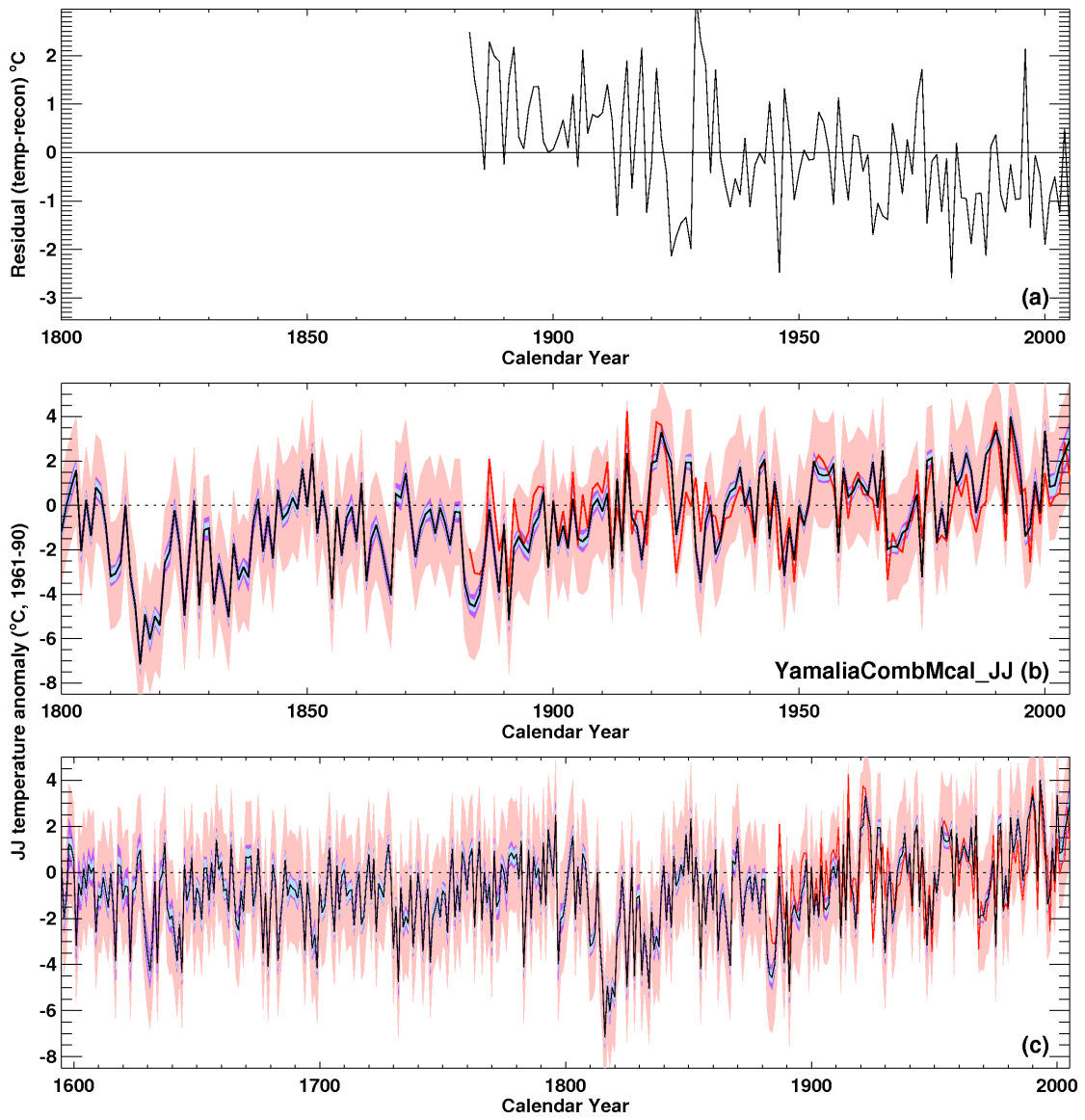


Figure ST06. As Figure ST04 but for JJ temperature.

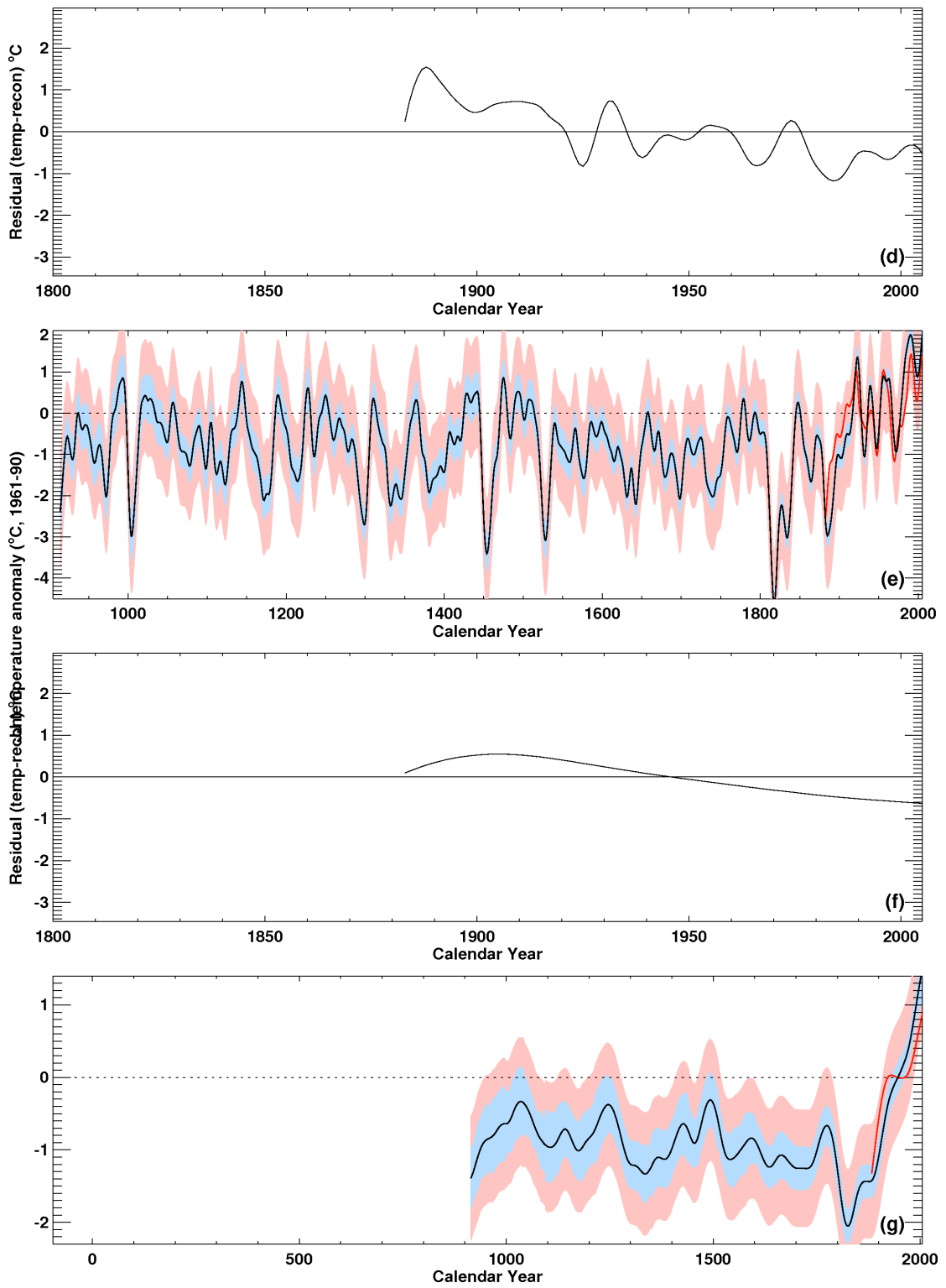


Figure ST06 (continued).